

Spatial and temporal variability of sound signals in shallow water with parameters varying in horizontal plane

Boris Katsnelson

School of Marine Sciences, University of Haifa, Israel

ABSTRACT

In the oceanic waveguide with parameters varying in horizontal plane (for example bathymetry - in area of coastal wedge, slopes and canyons, or in area of varying water layer - in the presence of nonlinear internal waves or temperature fronts, or in presence of both these effects) there is significant horizontal refraction or redistribution of the sound field in horizontal plane. Due to waveguide dispersion (dependence of modal propagation constants on frequency) it is possible to observe different spatial and temporal variations of the sound signal. It can be manifested in non stationary interference pattern, arrival time variations, variations of spectra etc. These effects can be used to solve different inverse problems especially by using horizontal and vertical line arrays.

INTRODUCTION

In the most publications, concerned with sound propagation in shallow water authors concentrated on the vertical variability of the temperature field, and discussed a simple model of how that variability arises. This vertical structure is the most important feature of the shallow water column, as the water column and bottom are approximately horizontally stratified (comprised of vertically stacked layers) over the propagation scales of interest, which reach to about 50 km in shallow water. However, horizontal stratification is a broad-brush first approximation only, and in many shallow water scenarios there is appreciable sound speed variability in the horizontal direction, as well as in the vertical. Perhaps the strongest horizontal variability in shallow water is due to shallow water fronts, bathymetry variations, mainly in area of coastal wedge and nonlinear internal waves. In given paper we consider just these three types of horizontal variability (stratification)

of the thermocline. Aforementioned temperature variations are accompanied by a change in the sound speed profile, which is most pronounced across the front. In the vicinity of the thermocline, the sound speed drop across the front can reach 15–20 m/s within a distance of several hundreds of meters. Such a difference corresponds to a substantial horizontal sound speed gradient, which persists over a rather large area. More detailed information on the temperature front is presented in Fig. 2: it shows a sequence of sound speed profiles in passing from one side of the temperature front to another in a region of the Barents Sea within a zone of about 500 m in length where the temperature variations are most pronounced [Jin et al, 1996, Lynch et al, 1996].

TEMPERATURE FRONT

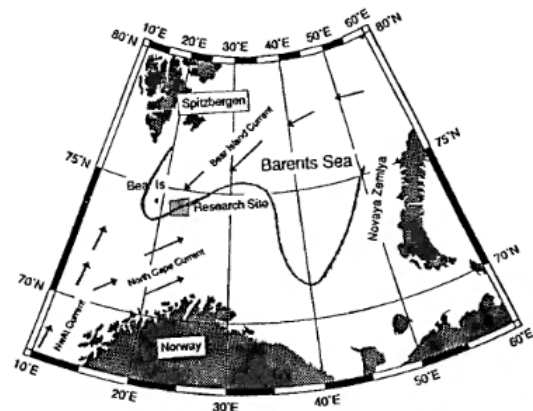


Figure 1. Temperature front (Barents sea Polar front)

Figure 1 shows the configuration of the Polar front in the Barents Sea [Jin et al, 1996]. The temperature variation is nonuniform in depth: as a rule, it is concentrated in the vicinity

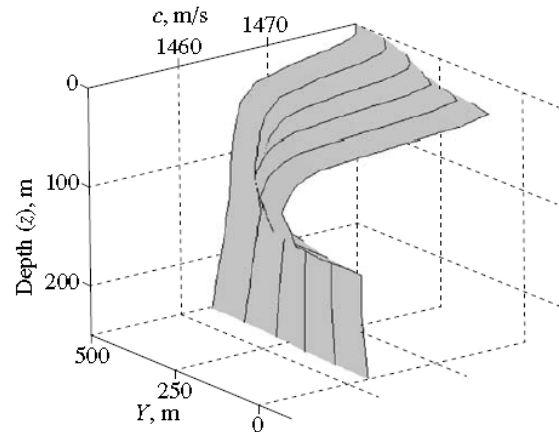


Figure 2. Sequence of the sound speed profiles in the vicinity of the temperature front. The nearest and farthest profiles correspond to the colder Arctic Current and the North- Atlantic Current, respectively

Under the influence of such a discontinuity, the oceanic medium becomes acoustically anisotropic, and a number of effects arise in the course of sound propagation through it. In particular, space-time fluctuations of the sound field due to the interaction of modes in the region where the acoustic path crossed the Polar front of the Barents Sea were considered in [Jin et al, 1996, Lynch et al, 1996]. Another effect that can considerably change the sound field is the horizontal refrac-

tion, which manifests itself when the acoustic path is approximately parallel to the TF. To such a phenomenon, the approach of horizontal rays and vertical modes can be applied. Such a study can reveal a number of spatial and frequency-time effects that, in principle, can be experimentally observed by using a vertical antenna array. In this sense, the influence of the temperature front on the sound field is similar to that of soliton-like internal waves (or internal solitons (IS)) [Katsnelson et al, 2011], although the horizontal gradients of the sound speed in the TF are 2–5 times lower than those in the IS, and the velocities of the TF are much smaller than those of the IS.

Let us consider the space-frequency features of the sound field propagating in a shallow-water sound channel with a temperature front. The oceanic medium is represented as a three-dimensional underwater waveguide in the Cartesian coordinate system where the (X, Y) plane coincides with the sea surface and the Z axis is directed vertically downwards. The waveguide is formed by the water layer $0 \leq z \leq H$ with density $\rho(x, y, z) = \rho_0(z) + \delta\rho(y, z)$ and a sound speed profile $c(x, y, z) = c_0(z) + \delta c(y, z)$, where $\rho_0(z)$ and $c_0(z)$ correspond to the profiles of density and sound speed on one side of the TF $y < 0$ in our case, δc and $\delta\rho$ characterize the variations of the acoustic parameters under the influence of the TF. The latter is considered to be plane and parallel to the X axis. The bottom is assumed to be homogeneous, liquid, and absorbing with density ρ_1 , sound speed c_1 , and absorption coefficient α . Here, the TF is modeled in such a way that, on average, the temperature (and the sound speed as well) at $y > 0$ is higher than that at $y < 0$ (see Fig. 2). Correspondingly, the horizontal rays leaving the source at $y < 0$ will be refracted in the same direction (Fig. 3). In other words, our statement of the problem corresponds to the situation where, at the receiving array positioned in the zone of intersection of horizontal rays, a complicated structure will be observed as the result of interference of the direct horizontal ray with a set of horizontal rays deflected by the temperature discontinuity and corresponding to different horizontal angles at the source and different vertical modes. The specificity of the horizontal refraction is that the horizontal rays corresponding to different frequencies and different vertical modes propagate along different trajectories, and, consequently, the intensity of the sound field at the aforementioned reception point may depend on the frequency and the ordinal number of the detected mode

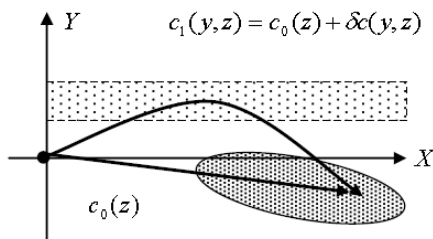


Figure 3. Schematic diagram of the horizontal refraction in the region near the temperature front. The shaded area is the zone of probable enhancement of the sound field due to horizontal refraction. The dashed strip approximately indicates the transition layer.

First of all, one can estimate the distance from the source and the temperature front, or, in other words, the position of the zone where one can expect the intersection of the direct and refracted horizontal rays and, hence, the manifestations of the aforementioned phenomena. Specifically, such a zone that is

closest to the source is determined by the maximum admissible departure angle β of the horizontal ray that returns to the region $y < 0$ after its refraction in the zone of the temperature front. In the simplest case, the estimate is as follows:

$$\beta \approx \sqrt{2 \frac{h_t}{H} \frac{\delta c}{c}} \quad (1)$$

Where h_t is the thickness of the thermocline. For the Barents Sea [Jin et al, 1996], $H \sim 230$ m, $h_t \sim 70-90$ m, $\delta c \sim 15-20$ m/s, and, hence, $\beta \approx 6-8 \times 10^{-2}$. This means that, if the source is at a distance of 600–800 m from the temperature front with a thickness of about 500 m, the effects of horizontal refraction manifest themselves at the receiver that is at a distance of about 20 km along the temperature front. Let us now consider the features of the sound field in this region

INTERNAL WAVES

Intense internal waves (IWs) are known to cause substantial perturbation of the low-frequency sound field. The well-known study [Rubinstein et al, 1991] reports on measuring the fluctuations of the sound field over a horizontal array in the presence of IWs with the propagation path passing at a small (about 10°) angle to the wave fronts of a train of intense IWs moving along the coastline. It was experimentally established that the amplitude fluctuations of the sound field correlated with the fluctuations of the water layer influenced by IWs. The data of

numerical simulation allow one to assume the adiabatic mechanism of interaction between the IWs and the sound field: the intensity variations are caused by local changes in the waveguide parameters. The tide-caused phase fluctuations of the sound field at a vertical array were studied in [Andreev et al, 1996]. A detailed study of fluctuations of the sound field under the influence of IWs was also performed in the SWARM'95 experiment [Apel et al, 1997] for different orientations of the acoustic path with vertical receiving arrays used for mode filtering. Publications [Badiy et al, 2002, 2005, 2007] devoted to analyzing the data of the SWARM'95 experiment show that, when the acoustic path is approximately parallel to the wave front of the IW train, intensity fluctuations can be rather substantial because of the influence of horizontal refraction. A theoretical analysis and estimation of intensity fluctuations were presented in [Badiy et al, 2007] in the framework of ray approximation in the horizontal plane. There, in terms of horizontal rays, the mechanism of intensity fluctuations was explained by changes in the ray density (the cross-section of the ray tube). In this case, the estimates of intensity variations can be obtained by assuming the horizontal rays to be approximately straight with perturbations of the

phase front being neglected. On the other hand, in the presence of an appreciable horizontal refraction, the objective of the studies consists in considering the fluctuations of the directions of sound propagation in the horizontal plane (the fluctuations of the phase front in a more general formulation), such fluctuations also taking place for the aforementioned orientation of the acoustic path. For instance, an experiment on measuring the fluctuations of the direction of sound propagation in the horizontal plane was carried out in the Barents Sea [Shmelev et al, 1992]. There, a horizontal antenna array was used to study the fluctuations in the phase distribution with characteristic periods starting from several tens of minutes, which, according to the authors, correspond to the typical periods of IWs.

In the present paper, we attempt to analyze the variations

of the sound-field phase front under the effect of a train of intense internal waves crossing the acoustic path and to estimate the possibility of experimental observation of such variations.

Illustration of influence on internal waves on sound propagation is shown in the Figure 3 where there is 3D shallow-water sound channel with IWs. The ocean medium is represented as an underwater waveguide in the XYZ coordinate system, where the XY plane coincides with the sea surface and the Z Axis is oriented vertically downwards. The waveguide is formed by a water layer $0 \leq z \leq H$ with a density $\rho(z)$ and a sound speed profile $c(x,y,z) = c_0(z) + \delta c(x,y,z,T)$, where $c_0(z)$ corresponds to the equilibrium stratification of the layer and $\delta c(x,y,z,T)$ characterizes the changes of the acoustic properties of the layer under the influence of IWs. The latter quantity depends on both coordinates and time T (we make a difference between the “slow” time T that characterizes the variability δc of the

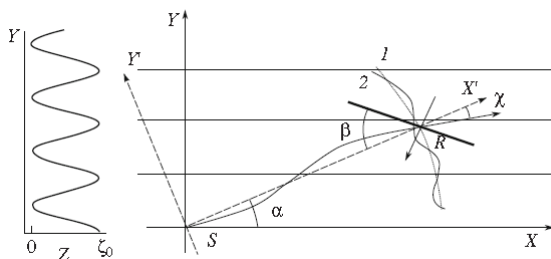


Figure 4. Statement of the problem. The XY coordinate system is related to IWs, the $X'Y'$ coordinate system is determined by the direction of the acoustic path, α is the angle between the path and the wave front of IWs, β is the angle between the path and the array, and γ is the angle of horizontal refraction. At the left, the position of the IW envelope is shown at the instant $T = 0$. The (1) dotted and (2) solid curves show the wave front without and with IWs, respectively.

Let us consider an IW train with an approximately rectangular wave front that is parallel to the X axis and with an envelope depending on the y coordinate and with an amplitude ζ_0 . This train propagates along the Y axis with a speed v (Fig. 1). The sound source S is located at the origin of coordinates in the horizontal plane $x = y = 0$ at a depth $z = z_l$. The transmitted signal is received at the observation point $R(x,y,z)$ by a horizontal array (usually, $z = H$). The initial position of the train envelope at $T = 0$ corresponds to that of the IW’s maximum at the source or to the zero shift of the train $vT = 0$ (the envelope with amplitude ζ_0 is shown in the left-hand part of Fig. 4). Because of slow propagation of the IW train, the characteristics of the sound field will depend on the position of the train, or on time T , in a parametric manner. For brevity, we do not write this dependence in an explicit form.

COASTAL WEDGE

In the ocean, coastal slope regions are of primary importance for both practical purposes and research, including acoustic studies. A typical coastal slope region has the form of a wedge with the angle between the sea surface and the bottom reaching $\sim 0.005\text{--}0.01$ rad; this region extends for several tens of kilometers (or more) from the coast to the shelf edge, where the sea depth is about 200–350 m. Beyond this line, the sea depth begins to increase steeply (the continental slope). In the theoretical studies of sound propagation, the coastal slope is usually described by a wedge-shaped model region with a constant velocity of sound and with ideally or nonideally reflecting boundaries [Dean et al, 1993, Jensen et al, 1980,

Pierce, 1982, Westwood, 1992]. The solution to the problem on the field in an ideal wedge can be constructed by using, e.g., imaginary sources, in analogy with the well-known Pekeris model; in this case, the imaginary sources are positioned in a circle [Westwood, 1992, Dean et al, 1993]. In some papers the field in the wedge is constructed in a cylindrical coordinate system (the z axis coincides with the edge of the wedge) based on modes depending on angle ϑ in the vertical plane. A somewhat different approach is possible in the case of a smooth dependence of the sea depth on the distance to the coast (a small slope), when the wedge-shaped region can be considered as a waveguide with varying depth and, in terms of the depth-dependent field expansion in modes, the field can be described in the adiabatic approximation (ignoring the mode coupling). In the two-dimensional version of the problem, where the field only varies in the vertical plane, one of the main features of sound propagation up the slope is the appearance of the critical cross section for a mode of a fixed number at a fixed frequency with decreasing depth and the reflection of this mode; or, the transformation of the mode in a leaky one and, hence, its escape to the bottom at a certain distance from the edge, this distance being different for different modes and frequencies [Buckingham, 1987]. The three-dimensional problem was considered in studies of the horizontal refraction of the acoustic field in a coastal slope region in both experimental (laboratory experiments [Tindle et al, 1987, Doolittle et al, 1988] and full-scale experiments in a coastal slope region [Doolittle et al, 1988]) and theoretical investigations. In the latter, the field behavior was described in terms of vertical modes and horizontal rays or numerically [Sturm, 2005] by a parabolic equation (see references in [Sturm, 2005]). For the ideal wedge model, the ray equations in the horizontal plane have analytic solutions describing the position and shape of rays and caustics in the form of hyperbolas. In this case, in a wedge with ideally reflecting surfaces, two rays (the direct ray and the reflected, or, refracted, one) arrive at each of the points of the horizontal plane, and the corresponding interference pattern is formed. We note that, for a more realistic model (a nonideal bottom, a coordinate-dependent sound velocity), the field pattern is more complicated, especially with allowance for the dependence of the refractive index of horizontal rays on frequency and vertical mode number. Sound propagation in the horizontal plane is similar to the propagation in an inhomogeneous dispersion medium with respective features for narrowband and broadband signals. Formally, a similar situation occurs in the vicinity of the temperature front [Katsnelson et al, 2007]. We note that analysis of the field structure can be used not only for the coastal wedge region itself,

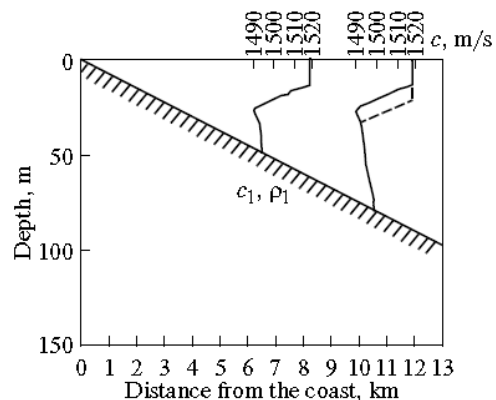


Figure 5. Bathymetry and sound velocity profiles for the waveguide model under study. The dashed line shows the perturbed sound velocity profile under mesoscale perturbation.

THEORY OF THE SOUND FIELD IN HORIZONTALLY STRATIFIED WAVEGUIDE

The complex sound field amplitude $P(\vec{r}, z, t)$ of a point sou- characterized by spectrum $S(\omega)$ and positioned at a point with the coordinates (x_s, y_s, z_s) is sought in the form

$$P(\vec{r}, z, t) = 2 \int_0^\infty \sum_l P_l(\vec{r}, \omega) \psi_l(\vec{r}, z; \omega) e^{-i\omega t} d\omega \quad (2)$$

Here, $\psi_l(\vec{r}, z; \omega)$ is the eigenfunction with the number l ; it is determined by the Sturm–Liouville problem and includes the dependence on r (or x, y) as a parameter; in addition, depends on frequency. The quantity $P_l(\vec{r}, \omega)$ which depends on the horizontal coordinates, the sound frequency, and the source coordinates, can be called the spectral mode ampli- tude.

We denote the corresponding eigenvalue (the longitudinal wavenumber) by $q_l(\vec{r}, \omega)$ and the transverse $\sigma_l(\vec{r}, \omega)$

For the value $P_l(\vec{r}, \omega)$ neglecting the mode coupling we can get two-dimensional Helmholtz equation

$$\nabla_\perp^2 P_l(\vec{r}, \omega) + q_l^2(\vec{r}, \omega) P_l(\vec{r}, \omega) = 0 \quad (3)$$

where $\nabla_\perp^2 = \frac{\partial^2}{\partial x^2} + \frac{\partial^2}{\partial y^2}$ is the Laplace operator in the hori- zontal plane.

Instead of the eigenvalue $q_l(\vec{r}, \omega)$, which determines the space and time dependences of the wavenumber for sound propagation in the horizontal plane, we introduce the cor- responding mode refractive index $n_l(\vec{r}, \omega) = q_l(\vec{r}, \omega) / q_l^0$

where q_l^0 is the eigenvalue of the transverse Sturm–Liouville problem; this eigenvalue corresponds to the cross section at a certain fixed point, e.g., at the point of the source position. We note that, in the region lying between the source and the coast ($y < y_s$), the wavenumber is $q_l < q_l^0$ and ($n_l(\vec{r}, \omega) < 1$). For a real situation, the latter index differs little from unity $n_l(\vec{r}, \omega) = 1 - \delta n_l, |\delta n_l| \ll 1$

Figures 6.7 shows the value of the refractive index for our models of temperature front and wedge as a function of the distance to front and to the edge of the wedge for different frequencies and mode numbers. One can see that, in the region $y < y_s$, the increment increases with an increase in the mode number and with a decrease in frequency; i.e., the refractive index in- creases with increasing frequency.

The frequency dependence of the refractive index makes the two-dimensional propagation medium a dispersion one (Eq. (2)). For such a medium, the evolution of the sound signal in time is determined by Eq. (1). If the spectrum of the emitted signal is sufficiently narrow, we can ignore the frequency dependence (which is sufficiently smooth) of the eigenfunc- tions within this spectrum; then, we factor out the eigen func- tions from under the integral in Eq. (1) at the central frequen- cy ω_0 of the source spectrum. In this case, the signal ampli- tude takes the form

$$P(\vec{r}, z, t) = 2 \sum_l \psi_l(\vec{r}, z; \omega_0) \int_0^\infty P_l(\vec{r}, \omega) e^{-i\omega t} d\omega = \sum_l \psi_l(\vec{r}, z; \omega_0) P_l(\vec{r}, t) \quad (4)$$

where the quantity $P_l(\vec{r}, t)$ can be interpreted as the pulse amplitude of the l -th mode. For a two-dimensional dispersion medium, we can write the wave equation

$$\nabla_\perp^2 P_l(\vec{r}, t) - \frac{1}{(c_l^0)^2} \frac{\partial^2}{\partial t^2} \hat{M} P_l(\vec{r}, t) = 0 \quad (5)$$

where $c_l^0 = \omega / q_l^0$ is phase velocity of the l -th mode, \hat{M} is nonlocal operator:

$$\hat{M} u = \int_{-\infty}^t \varepsilon_l(\vec{r}, t - t') u(\vec{r}, t') dt' \quad (6)$$

Eigen values can be expressed through dielectric permittivity

$$q_l^2(\vec{r}, \omega) = (q_l^0)^2 n_l^2(\vec{r}, \omega) = (q_l^0)^2 \varepsilon_l(\vec{r}, \omega) \quad (7)$$

Solution of wave equation can be found in the form of ray optics:

$$P_l(\vec{r}, t) = A_l(\vec{r}, t) e^{i\Theta_l(\vec{r}, t)} \quad (8)$$

And for phase function (eikonal) we can get time dependent ray equations

$$(\nabla_\perp \Theta_l)^2 - \frac{\varepsilon_l(\vec{r}, \omega)}{(c_l^0)^2} \left(\frac{\partial \Theta_l}{\partial t} \right)^2 = 0 \quad (9)$$

Moving wave front is determined by expression $\Theta_l(\vec{r}, t) = const$

Examples of refraction index in horizontal plane for wedge and temperature front are shown in the figures

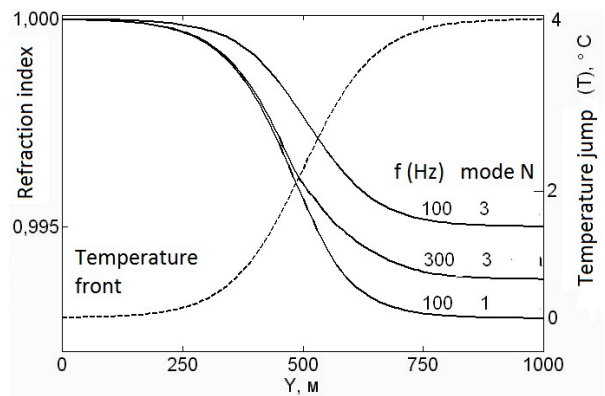


Figure 6. Dependence of the refractive index of the horizontal rays on the Y coordinate for some frequencies and mode numbers in the region of the temperature discontinuity. The dashed curve indicates the variation of temperature at some depth in the thermocline region across the temperature front

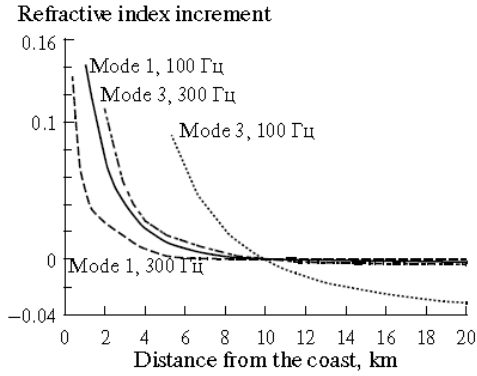


Figure 7. Dependence of the refractive index increment on the distance to the edge of the wedge for different modes and frequencies (the values are indicated in the plot)

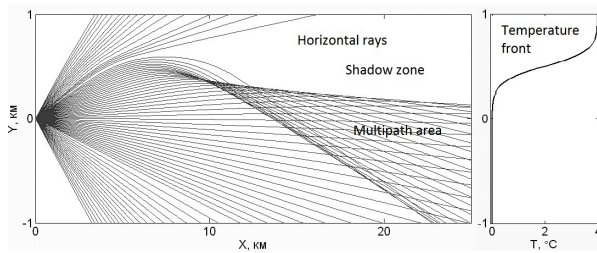


Figure 8. Ray pattern calculated by using the method of vertical modes and horizontal rays with the corresponding temperature distribution at some depth (at the right) in the vicinity of the temperature front for the first vertical mode at a frequency of 300 Hz.

If we take all the values $0 < t < \infty$, the corresponding curve will determine the spatial horizontal rays. Figure 8 shows examples of horizontal rays in area of temperature front. In the Figure we can see pattern of horizontal rays, in area of coastal wedge for a frequency of 100 Hz, which correspond to the first mode. In the plot, the multipath region can be distinguished. Its shape resembles a sector, so that, in what follows, we use the term “multipath sector” (MS). When the receiver is located in the MS, one should observe the interference of the direct and reflected fields of the corresponding modes if the overlapping of signals arriving over different ray paths takes place or if the signal doubling occurs with a certain time interval in the case of pulse arrival time measurements. The interference pattern is rather complicated because of the presence of regions where only one mode (the first) propagates or only two modes propagate (e.g., the first and second modes), and so on. The lower boundary of the sector, i.e., the boundary closest to the coast, represents the caustics (envelope) for the horizontal rays corresponding to a given mode and a given frequency, and the upper (limiting) horizontal ray indicates the MS boundary farthest from the coast. The positions of the boundaries can be estimated on the basis of a three-dimensional ray consideration with the use of the Brillouin (vertical) grazing angle β_l for the l th mode. The upper limiting ray path in the horizontal plane, or the horizontal launch angle of the boundary ray, which is denoted by (see Fig. 9a) and determines the aforementioned ray path, is governed by the parameters of the bottom or, more precisely, by the angle of total internal reflection from the bottom. As the ray propagates from the source, both the horizontal angle and the Brillouin angle of the given mode (the vertical grazing angle with respect to the bottom) β_l vary (Fig. 9b). In other words, during propagation up the slope (the channel narrows), the angle decreases, whereas the vertical grazing angle β_l , which depends on the local depth of the channel,

increases and, at a certain instant, may become identical to the angle of total internal reflection from the bottom which depends on c_1 . In this case, the direct ray penetrates to the bottom and the reflected (or refracted) ray is absent. The corresponding horizontal ray launch angle (see Fig. 3a) is determined as follows. The local eigenvalue corresponding to the total internal reflection, or the related bottom grazing angle of the Brillouin ray belonging to the l th mode is determined by the expression $\beta_l = \arccos(k_1/c_l)$ where $k_1 = \omega/c_1$ is the sea depth at the turning point. This yields the refractive index at the turning point for the horizontal boundary ray: $n = c_1/k_1$ where $k_1 = \omega/c_1$ and the horizontal angle at the turning point is zero. Then, \bar{x}_l is determined by the relation $\bar{x}_l = y_0 \frac{\sin \bar{\chi}_l \cos \bar{\chi}_l \cos^2 \beta_l^0}{1 - \cos^2 \bar{\chi}_l \cos^2 \beta_l^0} = y_0 \frac{k_1 \sqrt{(q_l^0)^2 - k_1^2}}{k^2 - k_1^2}$. The corresponding boundary ray path is shown in Fig. 9a. Now, we estimate the coordinates of the ray turning point (\bar{x}_l, \bar{y}_l) , which approximately coincides with the vertex of the MS under the assumption that the sound velocity in the wedge is constant. In this case, the horizontal ray paths and ray caustics have the form of hyperbolas [1, 4–6], whose equations are obtained in an analytic form. Using these results, for the coordinates of the vertex of the hyperbola corresponding to the boundary ray, we derive

$$\bar{x}_l = y_0 \frac{\sin \bar{\chi}_l \cos \bar{\chi}_l \cos^2 \beta_l^0}{1 - \cos^2 \bar{\chi}_l \cos^2 \beta_l^0} = y_0 \frac{k_1 \sqrt{(q_l^0)^2 - k_1^2}}{k^2 - k_1^2} \quad (10)$$

$$\bar{y}_l = y_0 \frac{\sin \beta_l^0}{\sqrt{1 - \cos^2 \bar{\chi}_l \cos^2 \beta_l^0}} = y_0 \frac{\sqrt{k^2 - (q_l^0)^2}}{\sqrt{k^2 - k_1^2}}$$

For our bottom model (the parameters are given above), we can assume that, in the denominator of Eq. (10), $q_l^0 \sim k$;

then, we have $\bar{x}_l \sim y_0 k_1 / \sqrt{k^2 - k_1^2} \sim 2y_0 \sim 20$ km. We see that \bar{x}_l weakly depends on both mode number and frequency. As for \bar{y}_l , this coordinate exhibits a more pronounced dependence on the mode number, as well as on frequency. For example, for the second mode at a frequency of 100 Hz, from Eq. (10) we obtain $\bar{y}_l \sim 0.5y_0 \sim 5$ km. In general, the straight line determines the boundary beyond which the l th mode does not propagate (at the given frequency). Figure 4 shows the MSs for the first two modes and frequencies of 100 and 500 Hz.

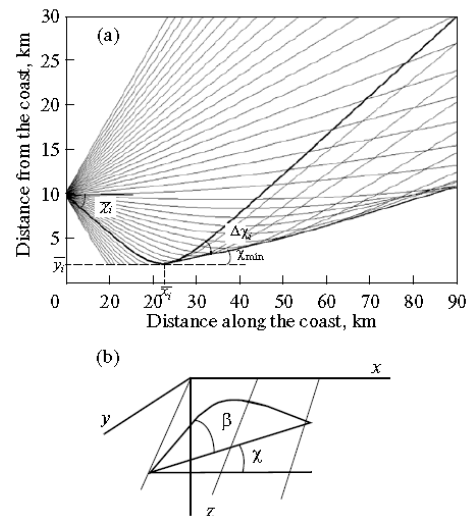


Figure 9. (a) Horizontal ray pattern for the first vertical mode at a frequency of 100 Hz; the solid lines indicate the MS. (b) The vertical and horizontal angles for a three-dimensional ray.

One can see that the numerically calculated position of the MS vertex approximately coincides with the coordinates determined above. If we assume that, for our wedge model,

the caustic approximately coincides with the asymptote of the corresponding hyperbola (the caustic for the case of a constant velocity), the slope of this asymptote is $\tan \beta_l^0$ i.e., its angle with the x axis is β_l^0 . This angle noticeably increases with increasing mode number. The asymptote of the “upper” horizontal boundary ray has the slope

$$\frac{dy}{dx} = \frac{\sqrt{k^2 - k_1^2}}{k_1}$$

which, in the framework of the simple model, is the same for different modes and frequencies and only depends on the sound velocities in water and in the bottom. In the case under consideration, the aforementioned estimate yields a slope of ~ 0.53 or an angle $\bar{\chi}_l \sim 30^\circ$, which approximately coincides with the numerical results represented in Figure 9a. In Fig. 9a, the direction of the lower boundary is determined by the angle χ_{\min} , which in our case approximately coincides with χ_{\min} for the first mode at a frequency of 100 Hz, this angle is $\chi_{\min} \sim 5^\circ - 6^\circ$. The vertex angle of the sector is estimated as and decreases with the mode number. We note that, as the mode number increases and the frequency decreases, the increment of the horizontal refractive index increases and the MS shifts toward greater depths. In this case, the characteristic spatial dimensions of the region vary (the transverse size of the MS at a distance of ~ 30 km makes about 2–4 km). As the frequency increases, the angle χ_{\min} decreases (tends to zero) and the lower boundary of the MS shifts toward the coast for all of the modes. From Fig. 4, where the MS boundaries are shown for frequencies of 100 and 500 Hz, one can see that the shift is fairly large: for the second mode, the lower boundary at a frequency of 500 Hz is 5–10 km nearer to the coast, as compared to the boundary position at a frequency of 100 Hz. The eikonal (the phase) taken at a certain point of the horizontal plane is determined by the phase velocity and the corresponding integral along the horizontal ray from the point of radiation to the point of reception (observation):

$$\Theta_l(M, t) = \int_{R_{0M}} q_l(x, y) ds \quad (11)$$

The characteristic features of the pulse arrival time are illustrated in Fig. 5, where, together with the horizontal ray pattern for the first and third modes at a frequency of 200 Hz, one can see lines lying in the horizontal plane, which correspond to a constant arrival time $t = 45$ s for signals propagating along the respective ray paths. The regions are denoted as follows: (I) the shadow zone for all modes, (II) the multipath region for the first mode and the shadow zone for the third mode, (III) the multipath region for the first and third modes, and (IV) the region of only the direct ray paths of these modes. One can see that, in the multipath regions, for each of the modes, there are two curves $t_l(x, y) = \text{const}$ corresponding to the direct and reflected signals. The signal propagating over the direct ray path goes farther within a fixed time interval as compared to the ray arriving over the reflected ray path. In other words, for a fixed point in the multipath region, the direct signal usually arrives earlier than the reflected signal; the difference decreases with decreasing distance to the caustics where the direct and reflected rays coincide. In our case, this quantity depends on frequency. The time of signal propagation over the ray path (which is an important observation characteristic) is determined by the integral along the ray path:

$$t_l(\omega) = \int_{R_{0M}} \frac{ds}{v_l^{gr}(\omega)} \quad (12)$$

where $v_l^{gr}(\omega)$ is the group velocity of the l th mode.

The characteristic features of the pulse arrival time are illustrated in Fig. 10, where, together with the horizontal ray pattern for the first and third modes at a frequency of 200 Hz, one can see lines lying in the horizontal plane, which correspond to a constant arrival time $t = 45$ s for signals propagating along the respective ray paths. The regions are denoted as follows: (I) the shadow zone for all modes, (II) the multipath region for the first mode and the shadow zone for the third mode, (III) the multipath region for the first and third modes, and (IV) the region of only the direct ray paths of these modes. One can see that, in the multipath regions, for each of the modes, there are two curves $t_l(x, y) = \text{const}$ corresponding to the direct and reflected signals. The signal propagating over the direct ray path goes farther within a fixed time interval as compared to the ray arriving over the reflected ray path. In other words, for a fixed point in the multipath region, the direct signal usually arrives earlier than the reflected signal; the difference decreases with decreasing distance to the caustics where the direct and reflected rays coincide. Comparing the arrival times at the reception point for different modes, we see that, in the absence of horizontal refraction (for the direct horizontal rays), a “conventional” order of mode arrivals is observed: the lower modes are usually characterized by a higher group velocity, and their travel time is shorter. For the reflected signals in region III, a different order of mode arrivals takes place. This change in arrival order is related to the fact that, despite the higher group velocity of mode 1, as compared to mode 3, the difference in the lengths of the respective ray paths is such that the order of arrival is changed. In particular (see Fig. 10), for the direct signal, the first mode arrives before the third mode (in regions III and IV), whereas, for the reflected signals (region III), the third mode arrives before the first one.

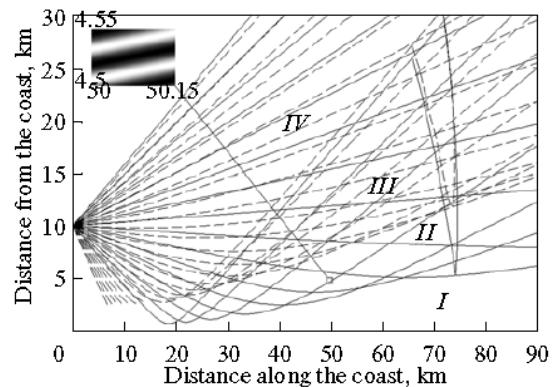


Figure 10. Multipath sector for the first two modes (the num_ bers are indicated at the right) and for frequencies of 100 (the solid line) and 500 Hz (the dashed lines) vertical modes. The frequency is 200 Hz. The lines lying in the horizontal plane and corresponding to a signal arrival time of 45 s are indicated. The inset shows the interference pattern formed in the horizontal plane segment near the point indicated in the plot.

Let us consider in more detail the signal arrival time at the observation point, which may fall within the MS. First of all remark that arrival times can be different for different horizontal rays, coming to the receiver. Typical values of arrival times are shown in the figure for temperature front, experimental observation of this effect was published in [Badiey et al, 2011] for moving forward front of internal waves. Next

we consider arrival times, as a function of frequency for different vertical modes (Fig.12). The corresponding pattern is called the frequency–time diagram and is often plotted in theoretical considerations and on the basis experimental data [Chen et al, 2003]. This pattern reveals the shapes of the dispersion curves for individual modes and is much used for solving various problems [Lopatka, 2010]. The position of the observation point used in our calculations is shown in Fig. 10 (its approximate coordinates are $x = 50 \text{ kmy} = 4.5 \text{ km}$). From Fig. 12 one can see that, for frequencies where $\omega_1 = 100 \text{ Hz}$, the receiver falls within the shadow zone for all of the modes. At the lower boundary of the MS shifts toward the x axis and the receiver falls within the caustic for the first mode; here, the direct and reflected rays coincide and the corresponding signals arrive simultaneously. With a further increase in frequency the lower

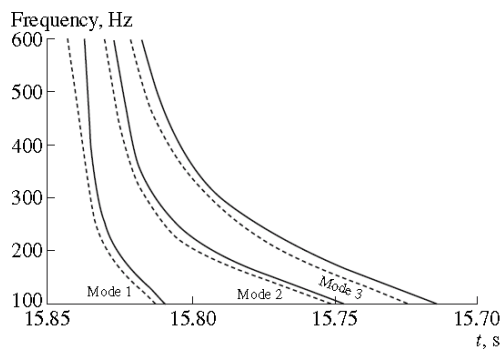


Figure 11. Arrival times for horizontal rays reflected from temperature front

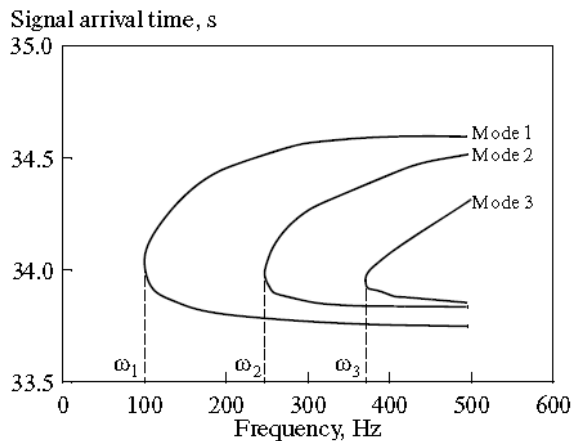


Figure 12. Frequency–time curves for three modes. The numbers are indicated in the plot.

boundary of the MS shifts further and falls within the MS for the first mode (still remaining in the shadow zone for the second mode); in this case, two signals are observed with the interval between the first mode arrivals over the direct and reflected ray paths increasing with frequency (the characteristic time between the direct and reflected signal arrivals is $\sim 0.5 \text{ s}$). This corresponds to zone II in Fig. 10. As the frequency increases, the signal travel time decreases for the direct ray (the group velocity increases with frequency) and increases for the reflected ray (because of the predominant increase in the ray path length). When the frequency reaches the value $\omega = \omega_2 \approx 250 \text{ Hz}$, the second mode appears at the observation point and the situation is reproduced. For a fixed

mode number, as the frequency increases further, the observation point may fall outside the multipath region (we denote the corresponding frequency value as ω) and, in this case, only one signal arrives at the observation point. Note that the specific values of ω and ω_c depend (in addition to the dependence on the waveguide parameters and the mode number) on the position of the observation point in the horizontal plane. The situation where the observation point falls outside the MS is only possible when this point lies in a relatively narrow region near the upper boundary (see Fig. 9). Such a frequency–time diagram can be plotted in experiment with the use of broadband signals (a frequency band of about 50–500 Hz). It is also possible to consider the spectral features of the signal and, in particular, the spectrum of the received signal as a function of the receiver position. These features are determined by the frequency dependence of the horizontal ray paths.

Work was supported by BSF, grant 2010471, and RFBR grant 12-05-00887

REFERENCES

Andreev M., Katsnelson B., Kulapin L., Petnikov V. 1996 Influence of hydrodynamic variability in shallow water on phase of the sound field. *Acoustical physics*, V.42(4) P.459-464

Apel J. R., Badiy M., Chiu C.-S., Finette S., Headrick R. H., Kemp J., Lynch J. F., et al. 1997. An overview of the SWARM 1995 shallow-water internal wave acoustic scattering experiment. – *IEEE J. Ocean. Eng.*, V22, , P. 465-500

Badiy M., Mu Y., Lynch J. F., Apel J. R., and Wolf S. N. 2002 Temporal and azimuthal dependence of sound propagation in shallow water with internal waves. – *IEEE J. Ocean. Eng.*, V.27, P. 117-129.

Badiy M., Katsnelson B.G., Lynch J. F., Pereselkov S.A., Siegmann W.L. 2005 Measurement and modeling of three-dimensional sound intensity variations due to shallow-water internal waves. – *J. Acoust.Soc.Am.*, V.117, N2, P. 613-625.

Badiy M., Katsnelson B. G., Lynch J. F., Pereselkov S. A.. Frequency dependence and intensity fluctuations due to shallow water internal waves. – *J. Acoust.Soc.Am*, 2007, V.119, N8, P. 747-760.

Badiy M. Katsnelson B. Y-T Lin, Lynch J. 2011 Acoustic multipath arrivals in the horizontal plane due to approaching nonlinear internal waves. *Journal of Acoust. Soc. Am.* , V.129, N4, EL141-147

Brekhovskikh L., Lysanov Yu. 2003, *Fundamentals of ocean acoustics*, 320 s

Buckingham M.J. 1987 Theory of three dimensional acoustic propagation in a wedge-like ocean with a penetrable bottom. // *Journal of Acoust.Soc.Am.*, V.82, N1, C.198-210

Burridge R. and Weinberg H. 1977 , in *Wave Propagation and Underwater Acoustics*, Ed. by J. B. Keller and J. S. Papadakis (Springer-Verlag, Heidelberg;)

Chen C, Miller J. H., Bourdreaux-Bartels G. F., Potty G. R., and Lazauski C. J. 2003 , “Time-frequency representations for wideband acoustic signals in shallow water,” in *Oceans-2003*, Sept., vol. 5, pp. 2903–2907

Dean G., Buckingham M. 1993. An analysis of the three dimensional sound field in a penetrable wedge with a stratified fluid or elastic basement. // *Journal of Acoust.Soc.Am.*, v.93(3) P. 1319-1328

Doolittle R., Tolstoy A. 1988. Experimental confirmation of horizontal refraction of cw acoustic radiation from a

- point source in a wedge-shaped ocean environment. // *Journal of Acoust.Soc.Am.*, v.83(6) 2117-2125
- Jensen F.B., Kuperman W. 1980 . Sound propagation in a wedge shaped ocean with a penetrable bottom. // *Journal of Acoust.Soc.Am.*, T.67, N5, C.1564-1566
- Jin G. and Lynch J., Chiu C-S, Miller J.H. 1996. A theoretical and simulation study of acoustic normal mode coupling effects due to the Barents sea Polar Front, with applications to acoustic tomography and matched-field processing. *J. Acoust. Soc. Am.* 100(1), P.193-205.
- Katsnel'son B. G, Lynch J., and Tskhoidze A. V. 2007, Space–frequency distribution of sound field intensity in the vicinity of the temperature front in shallow water. *Acoust. Phys.* **53**, 611-617.
- Katsnel'son B. G. and Tskhoidze A. V. 2008. Sound Field Phase Front Variations in Shallow Water in the Presence of Intense Internal Waves. *Acoustical Physics*, Vol. 54, No. 6, pp. 835–843
- Lopatka M., 2010, EURASIP J. Adv. Signal Proc. 2010, 1
- Katsnel'son B. G., Malykhin A. Yu., and Tskhoidze A. V., 2011 Rearrangement of the horizontal space–time structure of the sound field in shallow water in the presence of moving internal waves. *Acoust. Phys.* **57**, 368-375
- Lynch J. Jin G, Pawlowich R., Ray D., Pluedderman A.R. Bourke H.,Parsons A.R, Muenich R.. 1996 Acoustic travel time perturbation due to shallow water internal waves and internal tides in the Barents Sea Polar front: Theory and experiment. *Journal of the Acoust. Soc. Am.*, v.99(2), p. 803-821
- Pierce A. 1982 , Guided mode disappearance during upslope propagation in a variable depth shallow water overlying a fluid bottom. // *Journal of Acoust.Soc.Am.*, V.72, N5, C.523-531
- Rubenstein D., Brill M. N. 1991, Acoustic variability due to internal waves and surface waves in shallow water, in *Ocean Variability and Acoustics Propagation*, eds. J.Potter and A. Warn-Varnas (Kluwer Academic, Dordrecht.), Pp. 215-228.
- Shmelev A. Yu., Migulin A. A., Petnikov V. G. 1992. Horizontal refraction of low frequency acoustic waves in the Barents Sea stationary acoustic track experiment. – *J. Acoust.Soc.Am.*, 1992, V. 92, N2, P. 1003-1007
- Sturm F. 2005 Numerical study of broadband sound propagation in three-dimensional oceanic waveguide. // *Journal of Acoust.Soc.Am.*, v.117(3) P.1058-1079
- Tindle C.T., Hobaek H.,Miur T.G 1987 Downslope propagation of normal modes in a shallow water waveguide. // *Journal of Acoust.Soc.Am.*, V.81, N2, C.275-286.
- Westwood E. 1992 , “Broadband modeling of the three-dimensional penetrable wedge,” *J. Acoust. Soc. Am.*, V.92, P.2212–2222